Quantum Dice and the Delayed-Choice Quantum Eraser

Thomas V. Higgins

Abstract

This paper applies the mathematical metaphor of quantum dice to fully replicate the joint-detection data of the delayed-choice quantum eraser. The resulting theoretical plots closely match the symmetric and antisymmetric empirical data reported by Kim et al. in their original paper, but they also reveal an inconsistency with the single-slit joint-detection data presented in that same paper. These theoretical findings demonstrate the effectiveness of the stochastic quantum-dice interpretation for analyzing the delayed-choice quantum eraser.

Published by tvhiggins.com February 1, 2026

Introduction

My previous paper "Rolling the Dice on the Delayed-Choice Quantum Eraser" [1] introduced the quantum-dice interpretation of this famous experiment. By equating the experiment's results to the random outcomes of a pair of entangled quantum dice, I was able to reproduce the symmetric and antisymmetric joint-detection data presented by Kim et al. in their original paper. [2]

This supplemental paper further pursues that quantum-dice interpretation by using it to plot out the complete theoretical waveforms for all four joint-detection scenarios. Not only does the outcome graphically confirm a close match with the double-slit coincidence data originally reported by Kim et al., but it also reveals an unresolved incongruity with the single-slit coincidence data presented in Fig. 5 of that same paper. [2] I will discuss the nature of this incongruity and show why it is incompatible with their double-slit data.

The quantum-dice matrix

In my previous paper, I introduced the following quantum-dice matrix, which symbolizes all of the coincidence detections of the delayed-choice quantum eraser:

$$\begin{pmatrix} \Psi_1 D_1 & 0 & \Psi_3 D_1 & \Psi_4 D_1 \\ 0 & \Psi_2 D_2 & \Psi_3 D_2 & \Psi_4 D_2 \\ \Psi_1 D_3 & \Psi_2 D_3 & \Psi_3 D_3 & 0 \\ \Psi_1 D_4 & \Psi_2 D_4 & 0 & \Psi_4 D_4 \end{pmatrix}$$

Matrix 1

Each row of Matrix 1 lists those joint detections involving a specific idler detector (D_1, D_2, D_3, or D_4), while each column contains the specific wavefunction (Ψ_1, Ψ_2, Ψ_3, or Ψ_4) detected at the scanning detector D_0. The actual joint-detection rates appearing in this matrix depend on the location of D_0 as well as the specific wavefunction detected by D_0. These rates (intensities) are all calculated from the standard interference and diffraction effects of the slits.

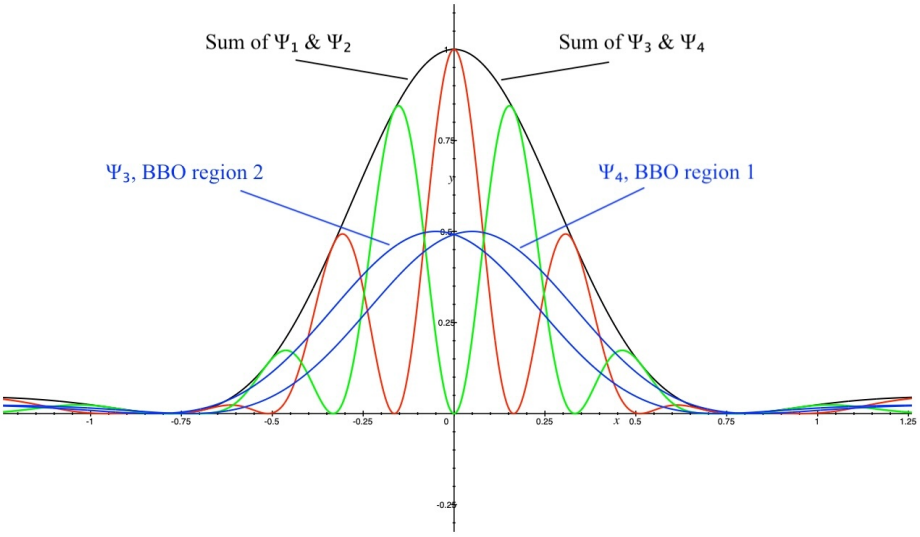

Figure 1

Figure 1 plots these calculated intensity curves for all four wavefunctions at arbitrary D_0 positions. The red and green plots represent the symmetric and antisymmetric double-slit wavefunctions (Ψ_1 & Ψ_2), and the blue plots depict the single-slit wavefunctions (Ψ_3 & Ψ_4).

Using Matrix 1 and Figure 1, we can compute the total joint-detection rates for wavefunctions that involve each idler detector—for example D_1 in matrix row 1. We simply add the average value of the off-diagonal elements of a specific matrix row to the diagonal element of that same row. In this way we account for the random "background" joint detections at the idler detector of interest. For D_1 this would be: $\Psi_1D_1 + (0 + \Psi_3D_1 + \Psi_4D_1)/3$. A similar formula applies to the remaining three matrix rows of Ψ_iD_2, Ψ_iD_3, and Ψ_iD_4. Refer to my previous paper [1] for the reason why one element in each row of Matrix 1 must be set to zero, and read my paper "Disentangling the Delayed Choice Quantum Eraser" [3] for a fuller description of the physics behind the delayed-choice quantum-eraser experiment.

Applying the quantum-dice matrix to the experiment

Figure 2 and Figure 3 show the actual joint-detection rates reported by Kim et al. for the symmetric and antisymmetric double-slit wavefunctions. Notice how their joint-detection curves ride above a conspicuous floor instead of going to zero where theory predicts in Figure 1. This

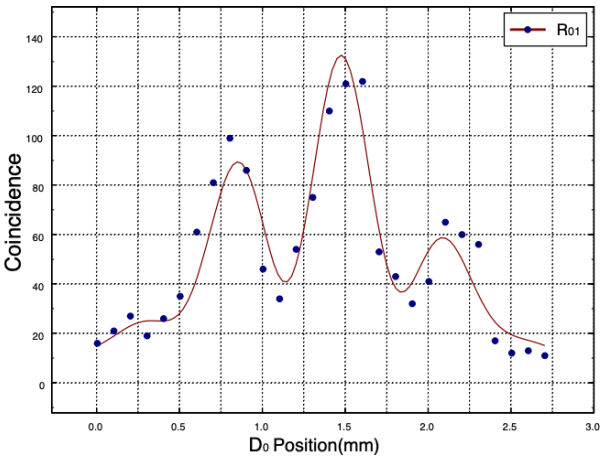

Figure 2 (from [2])

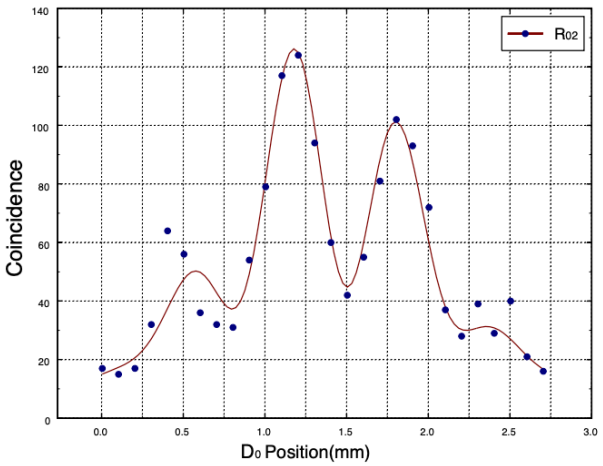

Figure 3 (from [2])

disparity results from an accumulation of the other random joint detections shown in rows 1 and 2 of Matrix 1. These include Ψ_3D_1, Ψ_4D_1 in row 1 and Ψ_3D_2, Ψ_4D_2 in row 2. Let's see what we get when we calculate these same two joint-detection rates (Ψ_iD_1 and Ψ_iD_2) using Matrix 1, Figure 1, and the summing formula I gave on the page above. (See Figures 4 & 5 below.)

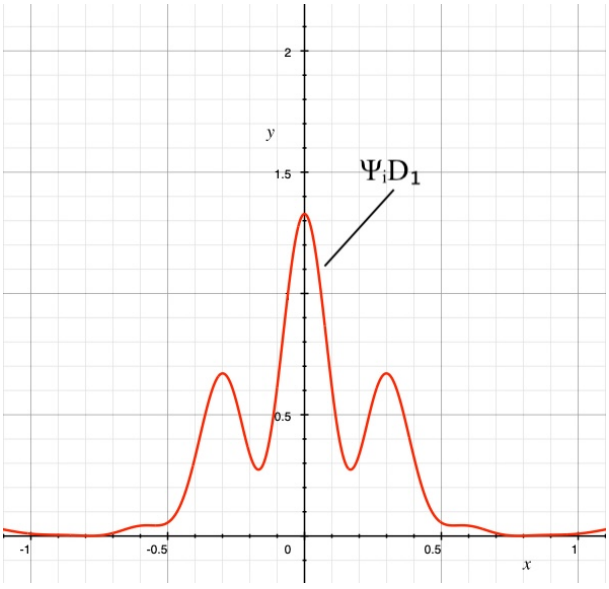

Figure 4

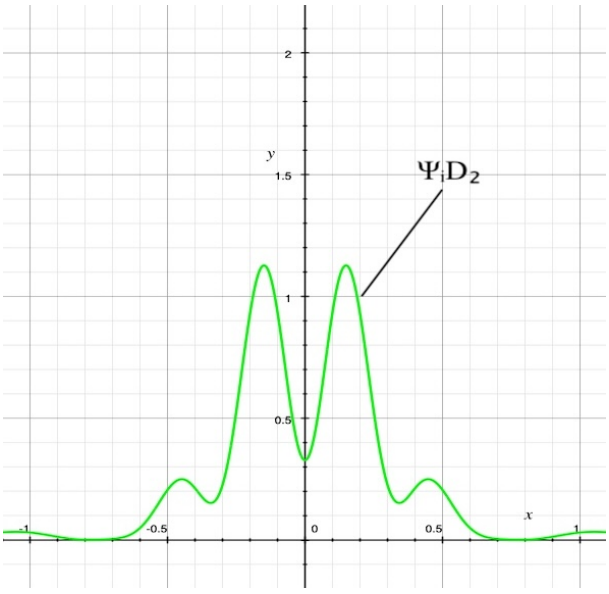

Figure 5

The empirical waveforms of Figures 2 & 3 are understandably not as symmetrical as the calculated curves of Figures 4 & 5, but their similarities are otherwise unmistakeable.

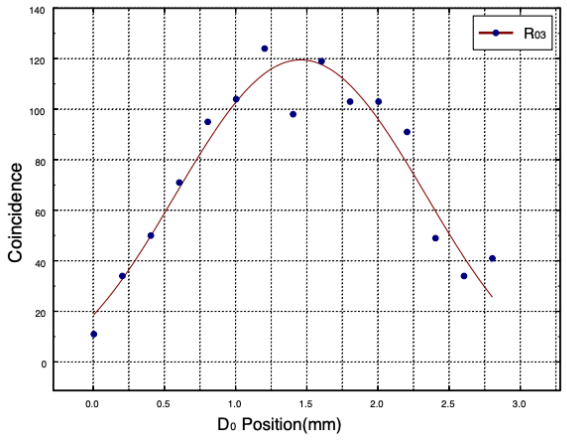

Figure 6 (from [2])

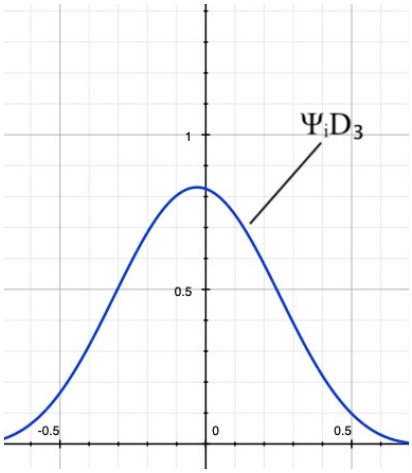

Figure 7

However, the single-slit joint-detection data reported by Kim et al. (Figure 6) has a noticeably higher maximum (~120) than the calculated maximum depicted in Figure 7 (0.83 x 100 = 83). Like the double-slit waveforms shown on the page above, the overall shapes of the single-slit curves in Figures 6 & 7 track well; unlike the double-slit data, their amplitudes do not. This is an incongruity among the data reported by Kim et al., not the calculated data. Figure 8 shows why.

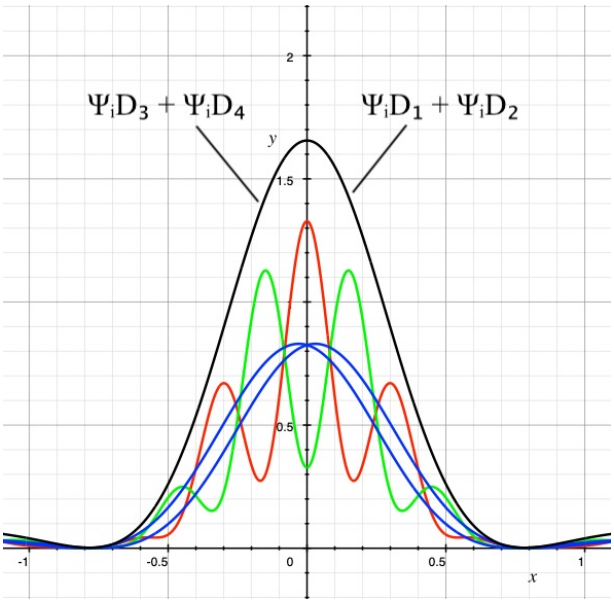

Figure 8

Figure 8 displays the calculated joint-detection curves involving D_0 and all four idler detectors ($\Psi_i D_1$, $\Psi_i D_2$, $\Psi_i D_3$, and $\Psi_i D_4$). Also included is a curve of the sums $\Psi_i D_1 + \Psi_i D_2$ (red curve + green curve) and $\Psi_i D_3$, + $\Psi_i D_4$ (sum of the two blue curves). Notice that these two sums trace the same black curve. Conservation of energy demands that they be the same. If Kim et al. also had included a D_0-D_4 joint-detection plot that matched the D_0-D_3 plot they did report (Figure 6), their sum would exceed the sum of D_0-D_1 + D_0-D_2 (Figure 2 + Figure 3). One can only speculate on the source of this incongruity. Perhaps the pump laser was pumping out more photons when they collected their D_0-D_3 data. Who knows? Their paper is silent on this, as it is on so many other particulars.

Conclusion

Entangled quantum dice offer a deeply instinctive and effective strategy for portraying the stochastic nature of the delayed-choice quantum eraser. Not only does it provide an insightful window into the utterly random behavior of this now famous experiment, it accurately replicates the joint-detection data, reveals an inconsistency within the originally reported data, and thoroughly refutes those upside-down “retrocausal” interpretations in which the present is somehow affecting the past.